Final Technical Report for DOE Award No. DE-FG02-05ER15671 University of North Carolina at Chapel Hill

March 7, 2023

Alan M. Jones

Dept Biology

University of North Carolina

Chapel Hill, NC 27599

Period of Performance: September 15, 2005 through June 14, 2022

This work was supported by a grant from The Division of Chemical Sciences, Geosciences, and Biosciences, Office of Basic Energy Sciences of the US Department of Energy through the grant DE-FG02-05ER15671 to A.M.J.

VPS26 Moonlights as an Arrestin-like Adapter for a 7-transmembrane RGS protein in *Arabidopsis thaliana*

Fei Lou[1], Meral Tunc-Ozdemir[1], Vaithish Velazhahan[2], Christopher G. Tate[2], and Alan M. Jones[1,3,*]

[1]Departmenof Biology, The University of North Carolina at Chapel Hill, Chapel Hill, NC 27599 USA, [2]MRC Laboratory of Molecular Biology, Francis Crick Avenue, Cambridge, UK, [3]Department of Pharmacology, The University of North Carolina at Chapel Hill, Chapel Hill, NC 27599 USA

ABSTRACT

Extracellular signals perceived by 7-transmembrane (7TM)-spanning receptors on the plasma membrane utilize a cytoplasmic adaptor that propagates signaling and initiates a feedback circuit for desensitization by removal of these receptors at the plasma membrane leading to desensitization to that signal. Signal (agonist) binding often evokes phosphorylation at the C-terminal tail of many 7TM G-protein-coupled receptors in animal cells which then recruits a cytoplasmic intermediate adaptor, β-arrestin, that sets in motion clathrin-mediated endocytosis (CME). Some 7TM receptors have agonist-induced phosphorylation and CME that do not involve β-arrestin, therefore it is unclear how these phosphorylated 7TM receptors are internalized. Arrestins, neither α– or β-types, are not encoded in the Arabidopsis genome, yet Arabidopsis cells have a well characterized signal-induced CME of a 7TM protein, Regulator of G Signaling 1 (AtRGS1). We show that a component of the retromer complex, VPS26, moonlights as an arrestin-like adapter. VPS26A and VPS26B form heterodimer instead of homodimer or monomer. flg22, a bacterium-derived signal that alerts plant cells of the presence of a potential pathogen, induces phosphorylation of AtRGS1 within a cluster of serines in its C-terminal tail, dimerization, and its CME. The phosphorylated C-terminal tail peptide binds to VPS26A/B heterodimer with greater affinity than the unphosphorylated peptide. We propose that VPS26 serves as an arrestin-like adaptor in the CME of AtRGS1 dimerization biased for VPS26 signaling.

Introduction

Membrane bound receptors receive external signals by specific ligand binding leading to a conformational change of the receptor that is propagated to cytoplasmic couplers and signal amplifiers [1]. Decreasing the receptor pool size on the membrane changes response behavior to become hyposensitive to the cognate signal [2-4] but also to propagate signaling originating at the plasma membrane [5-7]. Phosphorylation of specific serine clusters on the cytoplasmic C-terminus of GPCRs by receptor kinases (GRK) recruits arrestin proteins which consequently facilitates clathrin-assembly and the subsequent CME [8-10].

Mammalian arrestins are comprised of four unique proteins in two classes: visual (Arr2 and Arr3) and non-visual (Arr1 and Arr4) arrestins with each characterized according to binding specificity. Visual arrestins bind the GPCR Rhodopsin whereas non-visual arrestins, also known as β-arrestins, bind other GPCRs [8, 11]. β-arrestins are multifunctional endocytic adaptors [12] and signal transducers [13, 14]. Binding affinity of β-arrestins to the phosphorylated GPCR is dependent on a G Protein Coupled Receptor Kinase (GRK)-mediated phosphorylation cluster on the C-terminus[15]. Conformational changes of the GPCR C-terminus are mediated by β-arrestins to provide accessibility for subsequent association of clathrin and ADAPTER PROTEIN complex 2 (AP2) for clathrin-mediated endocytosis (CME)[8, 16]. Additionally, β-arrestins may have multiple conformational states to facilitate binding on different phosphorylation clusters or patterns on the C-terminus of receptors [9, 14, 17, 18].

GPCRs are not utilized in plant cells because the single canonical Gα subunit is self-activating [19-21]. Instead, the plant G protein complex is kept in its inactive state, in part, by a seven-transmembrane (7TM) REGULATOR OF G PROTEIN SIGNALING (RGS) protein [22, 23]. The prototype 7TM RGS protein is AtRGS1 from *Arabidopsis thaliana* [20]. AtRGS1 has a 7TM helical bundle with cytoplasmic and extracellular loops that model with high confidence like the GPCR helical bundle. Found in intercellular loop 2, there is weak homology with the cyclic AMP GPCR (cAR) in slime mold [20] but cAR has functions that are independent of G proteins because cAR is found in ancient organisms that lack G proteins [24]. As elaborated below, some, but not all, GPCR-specific residues in the 7TM helical barrel of class A GPCRs are conserved in AtRGS1. Also like GPCRs, AtRGS1 internalizes upon treatment with signals, notably a metabolic precursor to a sugar and a 22-amino acid peptide (flg22) released from bacteria flagella that is

perceived by the plant host to recognize the presence of a potential pathogen [25].AtRGS1 internalization after flg22 treatment is dependent on phosphorylation of specific serine residues on the cytoplasmic C-terminus by receptor-like kinases, BRASSINOSTEROID INSENSITIVE 1 (BAK1) and BOTRYTIS-INDUCED KINASE (BIK1) [26-29]. Discrimination of flg22 is by the BAK1 and FLAGELLIN-SENSITIVE 2 (FLS2) co-receptor complex [30, 31]

Watkins and coworkers [25] searched for arrestin-fold proteins that potentially act as arrestin-like adaptors in Arabidopsis. Human Vacuolar Protein Sorting (VPS) protein, specifically contains an arrestin-like fold and have high structural similarity with β-arrestins despite lacking any significant sequence similarity [32]. However, VPS26 is already well characterized as a subunit of the retromer complex where it recognizes cargo to traffick them from the endosomal space to the plasma membrane in humans [32-34] as well as in Arabidopsis [35]. Previous analysis of VPS26 function suggests a role in receptor trafficking in humans [33]. Three Arabidopsis VPS26 proteins: AtVPS26a (At5g53530), AtVPS26b (At4g27690), and AtVPS26-LIKE (At1g48550) have sequence similarity with vertebrate VPS26 and arrestin proteins [25, 32], providing a logical starting point for elucidating the AtRGS1 internalization mechanism. The CME of AtRGS1 requires both (VPS) proteins 26A and 26B implying that a heterodimeric VPS26 dimer is involved in AtRGS1 endocytosis [36]. VPS26 is homodimeric in the retromer [37].

flg22-induced CME of AtRGS1 requires phosphorylation at a cluster in the C-terminal tail [36]. This requires a functional G protein complex, clathrin, Adaptor Protein 2 (AP2), and BAK1/FLS2. Upon activation by flg22, receptor kinases flagellin-sensitive 2 (FLS2) rapidly recruits its co-receptor BAK1 (BRI1-associated receptor kinase 1) to form an active complex and initiates immune signaling. AtRGS1 is phosphorylated by BAK1 [27, 28] and by Botrytis-induced kinase 1(BIK1) [38], and phosphorylation triggers its dissociation from both FLS2 and from the G protein complex within 10 minutes [28]. This enables auto-activation of Gα protein, which then dissociates from the Gβγ dimer and the FLS2 receptor complex to promote immune signaling [28, 39]. We hypothesize that during this time, the VPS26A/B heterodimer act as an arrestin-like adaptor and interact with the AtRGS1 phosphorylated C tail where it dimerizes or oligomerizes AtRGS1 to initiate endocytosis. Activation of FLS2 by flg22 induces a BIK1/PBL-mediated phosphorylation of RGS1 at and around Ser428 and Ser431 to promote AtRGS1 dissociation from the FLS2-G protein complex [39-41].

Results and discussion

Comparison of 7TM barrel residues of RGS1 with animal GPCRs

As shown in **Figure 1A**, our model of AtRGS1 predicts with confidence a GPCR-like 7TM helical bundle with electrostatic interactions and an intracellular conserved RGS domain. The model predicts with less confidence the structure of a linker region between the 7TM bundle and the RGS catalytic domain nor the C-terminal tail, possibly because these are intrinsically disordered. The C-terminal tail near the distal end of the RGS domain contains a cluster of Ser/Thr phosphosites.

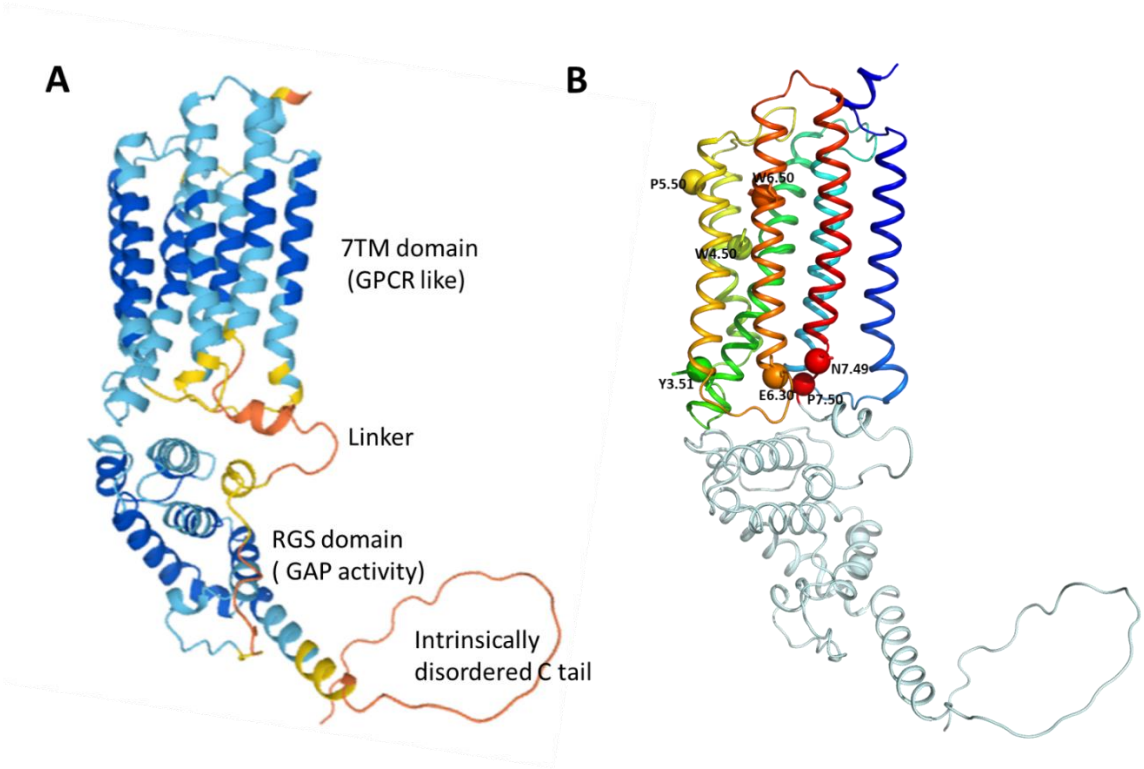

Figure 1. A, Alphafold2 model of RGS1. Model of RGS1 showed it consists of a 7TM domain and RGS domain connected by a linker, and an intrinsically disordered C tail. Model Confidence: Dark blue-Very high (pLDDT > 90) , light blue- Confident (90 > pLDDT > 70), orange - Low (70 > pLDDT > 50), yellow -Very low (pLDDT < 50). AlphaFold produces a per-residue confidence score (pLDDT) between 0 and 100. Some regions below 50 pLDDT may be unstructured in isolation. **B, conserved residues in 7TM bundle of RGS1**In each helix, the most conserved residues serve the starting points in the Ballesteros-Weinstein (B-W) residue numbering system(Ballesteros and Weinstein 1995). The most conserved residues in class A GPCRs are N1.50 in TM1, D2.50 in TM2, (D/E) R3.50Y, W4.50, P5.50, CWxP6.50 in TM6 and NP7.50XXY in TM7.

We compared the 7TM barrel residues of AtRGS1 with animal GPCRs. Class A GPCRs have conserved motifs with known class-specific functions [42]. In each helix, the most conserved residues serve the starting points in the Ballesteros-Weinstein (B-W) residue numbering system

[43] (Ballesteros and Weinstein 1995). The most conserved residues in class A GPCRs are N1.50 in TM1, D2.50 in TM2, (D/E) R3.50Y, W4.50, P5.50, CWxP6.50 in TM6 and NP7.50XXY in TM7. Motifs such as DRY in TM3, CWXP in TM6 and NPXXY in TM7 are acting as molecular switches. Mutations of key receptor residues involved in coupling to G proteins or β-arrestin reported resulting in biased receptor[44, 45]. For example, D2.50 is involved in GPCR activation while D2.50N point mutations are observed in GPCRs that show defective signaling. Highly conserved DRY/AAY biased receptors such as CXCR7, lack a typical sequence surrounding the DRY motif, thus no matter what ligand in the system, CXCR7 will only activate the β-arrestin signaling pathway [46-48].

Compared with the canonical motifs in Class A receptors, AtRGS1 has partially conserved motifs with several conserved point mutations similar with some GPCR-biased receptor (**Figure S1**). AtRGS1 conserved W4.50, W5.50 and P7.50 (**Figure 1B**). While conserved N1.50, D2.50 residues and CWXP and NPXXY motifs that are involved in GPCR activation are not present in AtRGS1. Interestingly, the residues of AtRGS1 QLY at the DRY motif in TM3 location is similar with the biased receptors of GPCR such as CRCX7 which can only activate the β-arrestin signaling pathway.

The C tail region of RGS1 is crucial for the binding between AtRGS1 and VPS26A/B

Using indirect quantitation, we showed previously that VSP26A and VPS26B interact with AtRGS1 at its cytoplasmic domain [36]. To test this directly and to quantitate the binding affinity though a direct assay, Microscale Thermophoresis (MST) quantitated binding of the phosphorylated and unphosphorylated AtRGS1 cytoplasmic domain and C tail (**Table 1**).

Table 1. Summary of the binding affinity tested using MST Summary of the binding affinity (Kd) among VPS26A and VPS26B with RGS1-C domain(J5), RGS1 C tail, pSer C tail, truncated pSer C tail, RGS1 C domain with C tail deletion (RGS1 J7). And the binding affinity (Kd) of VPS26A with VPS26B and VPS26B(Y85A/E93A) mutant. VPS26A/B means the heterodimer form of VPS26A and VPS26B. The values were determined from the binding isotherms shown in Figure S. The values are averages and StdDev for all the experimental replicates. Each experiment was replicated at least twice.

	RGS1 J5	RGS1 C tail	pSer C tail	Truncated pSer C tail	RGS1 J7	VPS26A	VPS26B	VPS26B (Y85A/E93A)
VPS26A	34 ± 6 nM	189 ± 58 nM		63 ± 43 nM	No binding detected	No binding detected	31 ± 8 nM	233 ± 53 nM
VPS26B	87 ± 2 nM	249 ±49 nM	39 ± 8 nM	82 ± 18 nM	No binding detected		No binding detected	
VPS26A/B		41 ± 21 nM	4.6 ± 4.2 nM					

The cytoplasmic domain of AtRGS1 (**RGS1 J5**, see **Figure 1A**) strongly bound VPS26A and VPS26B with affinities of Kd ~ 34 nM and ~87 nM, respectively (**Table 1**). This is similar in affinity to the AtRGS1 **J5** interaction with its Gα subunit partner AtGPA1 (125 ± 81 nM) [49]. The majority of the free energy for the interaction lies within the interface provided by the C tail because the RGS box without the C tail (**J7, Table 1**) showed no detectable binding and the synthetic C-tail alone bound to VPS26A and VPS26B at nM levels (Kd ~189 nM with VPS26A and 249 nM with VPS26B Fig. S3A) comparable to the affinity to **J5**. The raw data of the binding curves used to support the reported affinities of **Table 1** are provided in Supplemental Information **(Fig. S2-S6).**

We hypothesized that C-tail phosphorylation recruits VPS26s and, as such, the phosphorylated state has a higher affinity to VPS26. To map this interaction more finely, the last 10 residues of the tail were truncated without adverse effect on binding. The phosphorylated C tail bound VPS26A and VPS26 B ~3 times more than the unphosphorylated tail (**Table 1**, Kd ~63 nM with VPS26A and 82 nM with VPS26B Fig S3B).

VPS26A/B forms a heterodimer through the N domain beta sheet stacking between Y85 to E93 residues

Watson, et al (2021) used genetic and physical interaction *in vivo* to show qualitatively that VPS26 functions as a heterodimer [36]. We thus quantitated the Kd between VPS26A and VPS26B heterodimer and homodimer. As expected, the affinity between VPS26A and VPS26B was strong (Kd ~31 nM, **Table 1, Fig.S4A**) when using fluorescently-tagged VPS26A and VPS26B as the ligand. Interaction to form the VPS26A or VPS26B homodimers was not detectable (**Table 1**). This indicates that VPS26A and VPS26B are more likely to form a heterodimer than a homodimer

which is consistent with the previous *in vivo* BiFC, split luciferase, and genetic interaction data [25].

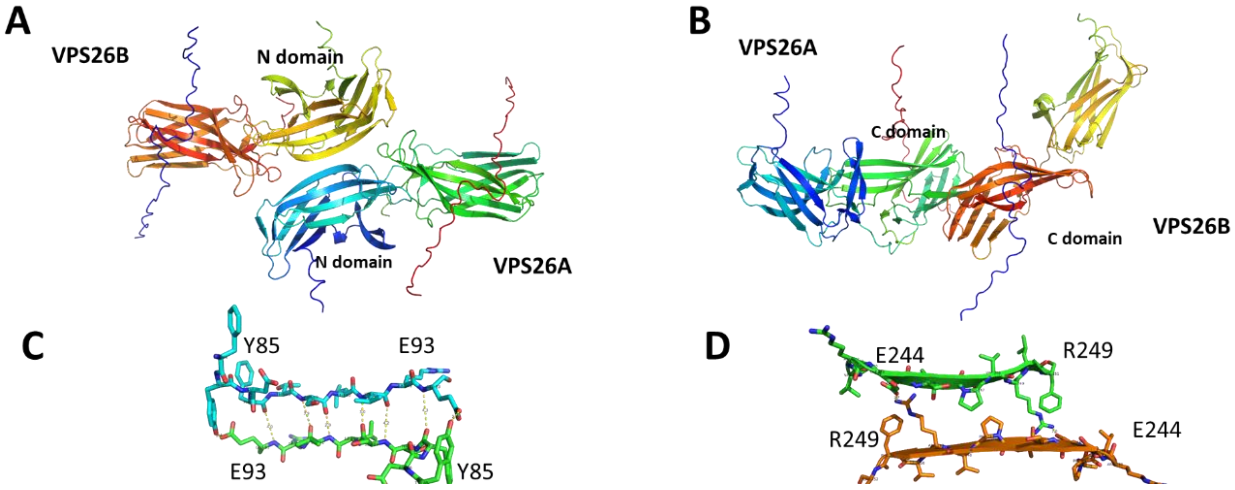

Figure 2. Alpha fold predicted model of VPS26 heterodimer with c tail (A) and phosphorylated C tail (B) and predicted interaction surface of VPS26A with VPS26B are showed in sticks and cartoon (C,D)

While there is a structure for the animal VPS26 homodimer in the retromer complex (PDB[7BLQ]), no structure is known for a plant VPS26A/B heterodimer. Therefore, a model was generated to show the potential binding pattern of the heterodimer of VPS26A with VPS26B (**Figure 2**). There are mainly two potential binding patterns showed by alphafold2 modelling: the N-domain and C domain beta-sheet stacking (**c.f. Figure 2A and 2B**). PRODIGY (see Methods) was used to predict the Kd of each model. The predicted Kd of the N domain stacking binding pattern was ~26 nM, similar to the experiment value, ~31 nM (**Table 1**). In contrast, the predicted Kd for C domain stacking binding pattern was ~1500 nM. Thus, both the *in silico* and experimental data suggests that VPS26A and VPS26B form a heterodimer by N domain, beta-sheet stacking.

Our model of the binding of the N-domain stacking predicts that the free energy change is largely due to the hydrogen bonds between Y85 to E93 (**Figure 2C**). This Y85-E93 region is highly conserved in both plant and animal VPS26 families. The VPS26 dimer crystal structure shows a similar binding surface between Y85 and E93 [37]. Based on our model and the animal VPS26 dimer interface, we generated a VPS26B Y85A/E93A point mutation and quantitated the Kd using MST. The VPS26B$^{Y85A/E93A}$ mutant heterodimerized ~8 times lower (Kd ~233 nM) compared to VPS26B WT (Kd ~31 nM) (**Table 1 and Figure S4B**). This further suggests that the

188 binding interface between VPS26A and VPS26B heterodimer is dominated by the hydrogen bonds
189 formed through Y85- E93 residues.

190 Mass photometry (MP) was performed to investigate VPS26A/B heterodimer formation *in*
191 *vitro* (**Figure 3A, Figure S8**). MP showed that VPS26A and the VSP26B mainly exists in
192 monomeric form with a near monodisperse peak at 53kD. At a 1:1 ratio of VPS26A and VPS26B,
193 mass photometry showed a monodisperse 107kD complex consistent with a heterodimer.

194

195 ***VPS26A/B heterodimer binds AtRGS1***

196 MP revealed that the VPS26/B heterodimer interacts with full-length AtRGS1 (**Figure 3B**).
197 Without VPS26, AtRGS1 together with its detergent form a 145-kDa particle. When the
198 VPS26A/B heterodimer is added, there the distribution of complex shifts to a higher weight but is
199 not monodisperse having an average mass of 223 kDa but larger particles are formed. To estimate
200 this binding affinity, we used MST with the truncated AtRGS1 proteins because MST is not
201 compatible with the detergents used to stabilize full-length AtRGS1. The labeled VPS26A -
202 VPS26B dimer was mixed as the target and the AtRGS1 C tail or pSer C tail were used as ligands.
203 The Kd between the AtRGS1 C tail and the VPS26A/B heterodimer was ~30 nM, ~3.5 times higher
204 than the Kd between the AtRGS1 C tail and VPS26A alone. The Kd between the AtRGS1 pSer C
205 tail also showed higher binding affinity towards the VPS26A/B heterodimer compared with
206 VPS26A alone (**Table1**). Thus, we generated a model of the complex of VPS26A/VPS26B
207 heterodimer interacting with AtRGS1 (Figure 3C). In this model, AtRGS1 is a dimer in the system
208 interacting with the VPS26A/VPS26B heterodimer.

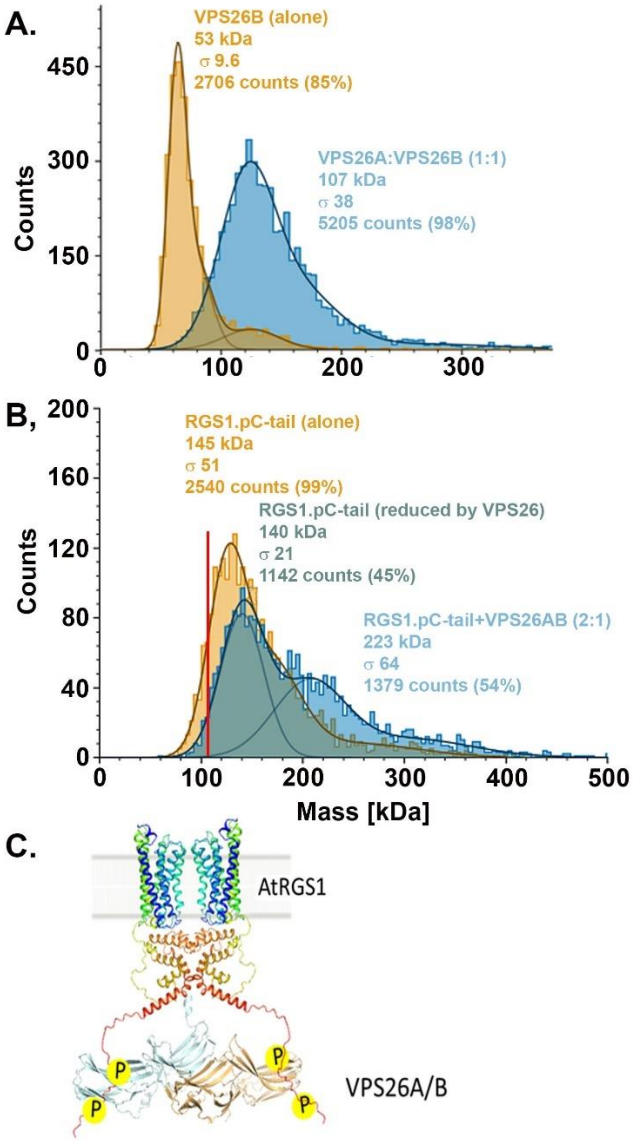

Figure 3. Mass photometry results of VPS26A/B and RGS1pCtail complex

Molecular mass distribution histogram of VPS26B and VPS26A/B complex(A) RGS1. pC tail and the complex of RGS1 with VPS26AB (B). The complex size increase when adding VPS26AB. RGS1 sample in 0.01% LMNG (10 CMC). Around 100 times dilution to around 0.1 CMC LMNG/CHS(1E-3 mM). Molecular weight of VPS26A: 50kD VPS26B: 50kD RGS1: 80kD RGS1-pCtail: 83kD pC tail: 3.5kD. The solid line represents major species fit with Gaussian functions. Width of the fitted peak (σ represents the standard deviation). Sum of the number of counts under the fitted peak expressed as the number of counts and the proportion of counts. (The proportion is defined as the number of counts compared to the total number of binding/unbinding events depending on whether the peak is located in the binding or unbinding domain of the histogram).VPS26B alone mainly exists in monomer form while VPS26A and VPS26B will form heterodimer when mixed together *in vitro*, which is consistent with MST results.Because each VPS26A or VPS26B has a binding interface with the AtRGS1 C tail, a valency of two is predicted to increase the affinity.

flg22 induce dimerization/ oligomerization of AtRGS1 3 S/A mutations inhibit flg22- induced RGS1 dimerization **[THIS SECTION NOT COMPLETED- figure is partially completed]**

VPS26 binds AtRGS1 and our model of the complex assumes that AtRGS1 is dimeric within this complex. We used an *in vivo* approach to test this. Using the Number and Brightness (N&B) method [50], a fluorescence microscopy method that is capable of measuring the apparent average number of molecules and their oligomerization (brightness) in each pixel from a series of fluorescence microscopy images. AtRGS1 exists mainly as a monomer (~%98.5) at resting state (**Figure 4A**). Two signals are known to induce AtRGS1 endocytosis: glucose and flg22, with flg22 acting through a clathrin-dependent pathway and glucose acting though a lipid raft pathway [25]. Glucose did not change the oligomerization state of AtRGS1 while flg22 induced dimer formation and increased the dimer percentage from 1.5% to 7.2% (Figure 4). This is likely a conservatively low value given the dynamics of the reaction and our ability to capture a change with the time resolution of this technique. The phosphor cluster described above is involved in the dimer formation.

Our previous data showed that loss of either VPS26A or VPS26B will reduce the flg22-induced CME pathway of AtRGS1 while no statistical effect on D-glucose–induced internalization of AtRGS1, suggesting that VPS26A/B dimers are involved in flg22, but not glucose–induced, AtRGS1 endocytosis [36].

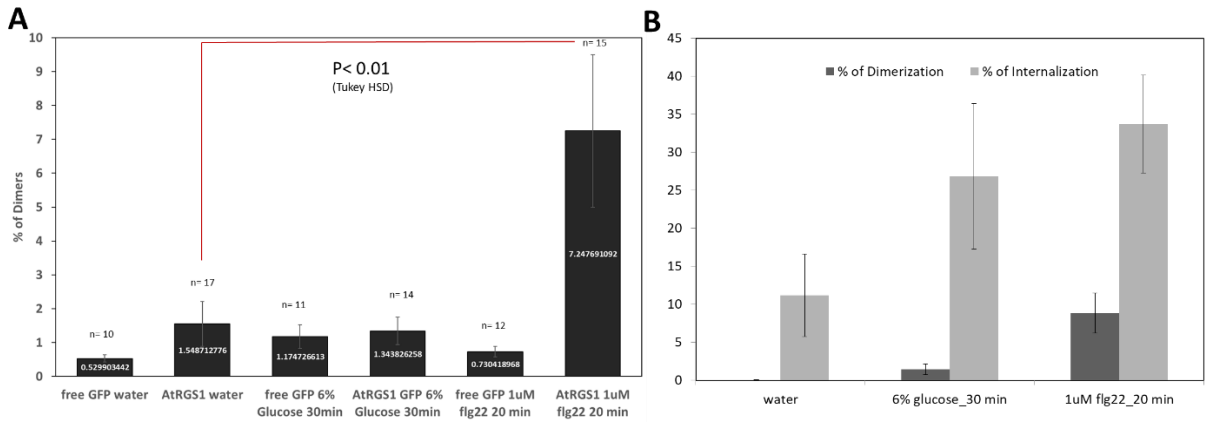

Figure4. oligomerization state of AtRGS1. AtRGS1 exists mainly as monomer (~%98.5 without a treatment). Flg22 induces dimer formation and increases the dimer percentage from %1.5 to %7.2. Glucose do not change the oligomerization state of AtRGS1.

Taken together both the *in vivo* and *in vitro* data, we are able to generate a predicted model of flg22-induce AtRGS1 endocytosis through VPS26 A and VPS26B heterodimer (Figure 5). In this model, flg22 will induce the phosphorylation and dimerization of RGS1. Thus, the phosphorylated dimer form of RGS1 will recruit the VPS26A/B heterodimer and then initiate the CME pathway of RGS1.

Whether the VPS26 heterodimer, drives oligomerization of RGS1.

RGS1 dimerization biased for VPS26 signaling? RGS1 dimerization in the presence of flg22/VPS26A/B (Split-luciferase). Interaction of VPS26A/B with RGS1 in the presence of flg22(Split-luciferase). Detect oligomerization state of RGS1 using VPS26A/B knock out system.

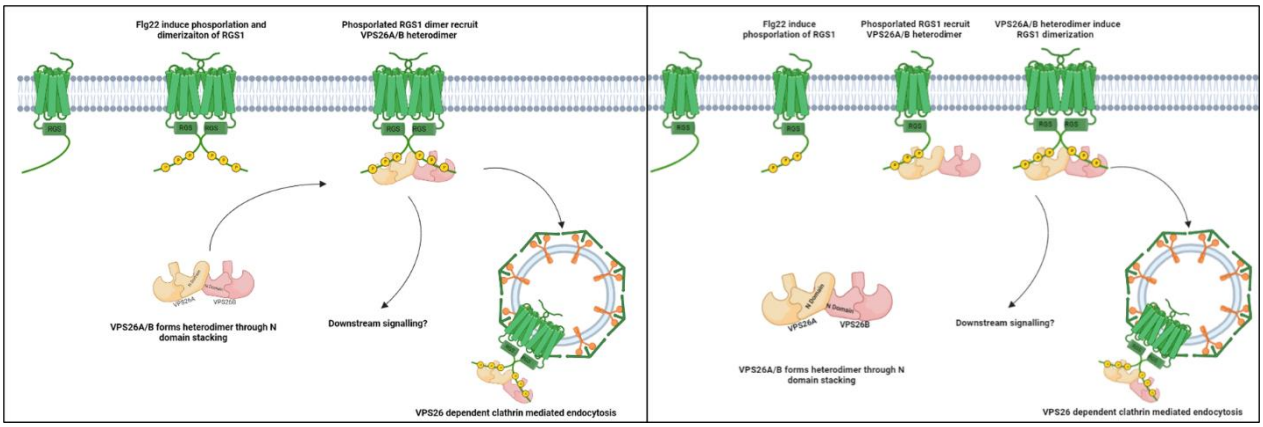

Figure5. Two potential models for flg22 induce RGS1 internalization RGS1 with VPS26AB RGS1 dimerization induced by flg22 or recruitment of VPS26 heterodimer? Detect oligomerization state of RGS1 using VPS26A/B knock out system. Whether RGS1 dimerization is associated with VPS26 heterodimer? In vitro test of RGS1 dimerization (Western blot) . In vivo test of whether RGS1 3 ser phosphorylation will enhance VPS26 binding. Flg22 induce atRGS1 phosphorylation on c tail . And phospho c tail recruit Vps26 heterodimer and thus dimerize RGS1 and induce CME pathway.

Conclusion

Taking the present data with the literature, we conclude, and to some degree, speculate that VPS2A and VPS26 B binds the 7TM RGS1 in a similar way as the hanging state of the GPCR- arrestin complex, in which the C domain convex region of VPS26A/B heterodimer, rich in positive charge, binds RGS1 through the phosphorylated C tail region. flg22 acts as the ligand to active the phosphorylation pathway through co-receptors BRASSINOSTEROID INSENSITIVE 1 (BAK1) and FLAGELLIN-SENSITIVE 2 (FLS2) [51], the phosphorylation of RGS1 C tail recruit VPS26A and VPS26B heterodimer. In this process, the RGS1 dimerization is triggered through the interaction of VPS26A/B heterodimer with RGS1 p-C tail (Ser428/431/435). VPS26 heterodimer will further recruit AP2 ADAPTOR PROTEIN COMPLEX-2 and clathrin to the complex and thus induce the clathrin-mediated endocytosis pathway. We propose that plant VPS26 is moonlighting as an arrestin-like adaptor in AtRGS1.

Materials and Methods

Modeling

Protein expression and purification

For protein expression, Plasmids contain 8 × His sumo-VPS26A and 8 × His sumo-VPS26B were transformed into BL21 (DE3) cells. Inoculate LB medium with Amp and grow overnight with constant shaking at 37°C. In large scale culture, inoculate with overnight culture (2% volume) in 1 L LB medium in 2.5 L flasks. Incubated at 37 °C, 225 rpm. At OD600 = 0.6 to 0.8, lower incubator temperature to 18 °C and grow for 30 min. Protein expression was induced using 0.5 mM IPTG at 18 °C for 16 h.

All purifications were performed at 4 °C. Cell pellets were resuspended in extraction buffer (25 mM Tris-HCl pH 8.0, 150 mM NaCl, 0.25 mg/mL Lysozyme, 1 × protease inhibitor cocktail, 5mM TCEP) and mixed for 30 min at 4 °C. The suspension was sonicated (Sonic Dismembrator, Model 550, Fisher Scientific, power level 5, 10s on and 20s off for 30 min) to disrupt the cells. The lysate was centrifuged at 30,000 × g for 40 mins, and then the soluble fraction was collected

and filter supernatant through 0.45μm vacuum filter. Then incubated with nickel resin for 30 min at 4 °C. Then resin was washed with washing buffer (extraction buffer above except with neither lysozyme nor thesit and adding 50 mM imidazole) and eluted with elution buffer (Washing buffer supplemented with 250 mM imidazole (Sigma-Aldrich)). The His-sumo tag was cleaved by ULP1 protease. Then go through a second time nickle column. The eluted proteins were run on size exclusion column (Superdex 200 10/300 GL, GE Healthcare) with running buffer (1 × PBS). Aliquoted protein samples were snap frozen by liquid nitrogen and store at −80 °C.

His-and GST-tagged RGS + Ct (AtRGS1, residues from 284 to 459) were cloned into pDEST15 destination vector as previously described (Li et al., 2016; Urano et al., 2012). RGS1 C tail deletion were cloned into PET 21b vector. Plasmids were transformed into ArcticExpress RP cells (Agilent Technologies). In large scale culture, 0.5 L LB medium in 2.5 L flasks were incubated at 37 °C, 225 rpm. At OD600 = 0.6 to 0.8, protein expression was induced using 0.5 mM IPTG at 12 °C for 16 h. All purifications were performed at 4 °C. Cell pellets were resuspended in extraction buffer (25 mM Tris-HCl pH 8.0, 150 mM NaCl, 2 mM MgCl2, 20 μM GDP, 5 mM 2-mercaptoethanol, 1 mM PMSF, 0.25 mg/mL Lysozyme, 0.1% Thesit (Sigma, 88315), 1 X protease inhibitor cocktail, 5mM TCEP) and mixed for 30 min at 4 °C. The suspension was sonicated 30 min (10s on and 20s off for 30 min) to disrupt the cells. The lysate was centrifuged at 30,000 X g for 40 mins, and then the soluble fraction was collected and incubated with Ni resin for 30 min at 4 °C. Then resin was washed with washing buffer (extraction buffer above except with neither lysozyme nor thesit and adding 50 mM imidazole) and eluted with elution buffer (Washing buffer supplemented with 250 mM imidazole). The eluted proteins were run on size exclusion column (Superdex 200 10/300 GL, GE Healthcare) with running buffer (20 mM Tris-HCl, pH 7.5, 50 mM NaCl, 10 mM MgCl2, 5mM TCEP). Aliquoted protein samples were snap frozen by liquid nitrogen and store at −80 °C. The His-GST tag was cleaved by TEV protease.

Mass photometry

All data was acquired using a OneMP mass photometer (Refeyn Ltd, Oxford, UK) Microscope coverslips (No. 1.5, 24 × 50 and 24 × 24 mm2, VMR) were cleaned by sequential sonication in 50% isopropanol (HPLC grade)/Milli-Q H2O, and Milli-Q H2O (5 min each), followed by drying with a clean nitrogen stream. Fresh aluminium foil was folded around an A4 size cutting board.

Individual 24 × 24 coverslips were taped using two strips of double-sided tape and cut from the foil using a scalpel blade. Each excised 24 × 24 coverslip was joined, tape side down, in the center of a 24 × 50 coverslip and stored prior to use.

Immediately prior to mass photometry measurements, protein stocks were diluted directly in stock buffer (unless stated otherwise). Typical working concentrations of protein complexes were 5–25 nM, depending on the dissociation characteristics of individual assemblies. Each protein was measured in new flow-chambers (i.e., each flow-chamber was used once). To find focus, fresh buffer was first flowed into the chamber, the focal position was identified and secured in place with an autofocus system based on total internal reflection for the entire measurement. For each acquisition, 15 µL of diluted protein was introduced into the flow-chamber and, following autofocus stabilization, movies of either 60 or 90 s duration recorded. Each sample was measured at least three times independently ($n \geqslant 3$).

Quantitative binding analyses by microscale thermophoresis (MST)

Measurements for equilibrium binding were performed using 20 nM fluorescence-labelled protein using Monolith NTTM Protein Labeling Kit RED-NHS and RED-MALEIMIDE (Nanotemper Technologies). The dye/protein ratio used was 10:1. Experiments were conducted at 25 °C and in 'MST Buffer' [PBS pH 7.4, 0.05% Tween-20]. Protein sample was centrifuged for 30 min (21,000 × g, 4 °C) before experiment. For thermophoresis measurements, ligand and labeled protein sample was mixed 1:1 with each of the ligand dilution series. After 10-min incubation at room temperature, each dilution was filled into Monolith NTTM MST Premium-coated capillaries (Nanotemper Technologies). A capillary scan was performed with 40% LED power. Binding curves were fitted to two sets of replicates. For binding experiments, Kd values were calculated via the MO. Affinity Analysis V2.3 software. This software performs a quality control based on the levels of starting fluorescence, and the distribution of the signal within the capillaries, an indicator of non-specific binding. A signal to noise ration above 5 provides high confidence of the data.

Plant growth

Stably transformed Arabidopsis lines expressing GFP-tagged AtRGS1 behind cauliflower mosaic viral (CaMV) 35S constitutive promoter (35S: AtRGS1-GFP), 35S: GFP, 35S:AtRGS1-YFP, or 35S:AtRGS1(3SA)-YFP reporter were sterilized and then stratified in 1-ml liquid ¼ MS medium without sugar at 5°C for 2 days. After they were treated for 2 hours with light, seeds were covered with aluminum foil and kept in darkness at room temperature for 5 days.

Imaging

Elongated hypocotyls were imaged using a confocal laser-scanning microscope (Zeiss LSM 880, http://www.zeiss.com/) with a C-Apochromat 40×/1.2 NA water immersion objective where GFP is excited at 488-nm. Hypocotyls were mounted on slides in water which was replaced with a solution of either water, 6% d-glucose, or 1 um of flg22 and imaged at 0, 30 and 20 minutes respectively.

Imaging according to the Number and Brightness technique (N & B)

The 256 x 256 pixel regions of interest on hypocotyls were raster scanned with a pixel dwell time of 4.12 us for 100 frames with a pixel size of 100 nm according to RICS image acquisition techniques. N&B analysis was first performed on Arabidopsis hypocotyls expressing Green Fluorescent Protein (GFP) driven by the CaMV 35S constitutive promoter (35S: GFP) to calculate the monomer brightness and cursor size as described in [52].

Analysis of the raster scans acquired for N&B

N&B uses the average fluorescence intensity, and the variance in fluorescence, to determine the brightness of particles and their number in an image thus establish the oligomeric state of proteins[50, 52]. The SimFCS software (https://www.lfd.uci.edu/globals/) was used for the analysis of the raster scans acquired for N&B. The background region of the image was normalized and monomer brightness is determined with the 35S:GFP or 35S:YFP lines. A cursor was used to cover all the pixels in the brightness versus intensity graph. The y-position of the cursor is used to calculate the brightness of the fluorescent protein. The cursor was positioned at the brightness value of monomeric protein. Any pixels within this cursor are monomers. Another cursor of the same size is placed on top of the monomer cursor. Pixels that fall inside this box are homodimers. The percentage of monomer was calculated by dividing the number of monomer pixels by the sum

of the pixels of all oligomeric forms (monomer plus homodimer). This was repeated to determine the percentage of homodimer forms.

References

1. Hanyaloglu, A.C. and M. von Zastrow, *Regulation of GPCRs by endocytic membrane trafficking and its potential implications.* Annual Review of Pharmacology and Toxicology, 2008. **48**(1): p. 537-568.
2. Pierce, K.L., R.T. Premont, and R.J. Lefkowitz, *Seven-transmembrane receptors.* Nat Rev Mol Cell Biol, 2002. **3**(9): p. 639-50.
3. Violin, J.D. and R.J. Lefkowitz, *Beta-arrestin-biased ligands at seven-transmembrane receptors.* Trends Pharmacol Sci, 2007. **28**(8): p. 416-22.
4. A., L., *The beta-adrenergic receptor and its mode of coupling to adenylate cyclase.* CRC Crit Rev Biochem. , 1981. **10 .**(2): p. 81-112.
5. von Zastrow, M., *Mechanisms regulating membrane trafficking of G protein-coupled receptors in the endocytic pathway.* Life Sciences, 2003. **74**(2-3): p. 217-224.
6. Lefkowitz, R.J., et al., *G-protein-coupled receptors: regulatory role of receptor kinases and arrestin proteins.* Cold Spring Harb Symp Quant Biol, 1992. **57**: p. 127-33.
7. Kahsai, A.W., B. Pani, and R.J. Lefkowitz, *GPCR signaling: conformational activation of arrestins.* Cell Res, 2018. **28**(8): p. 783-784.
8. Gurevich, E.V., J.L. Benovic, and V.V. Gurevich, *Arrestin2 expression selectively increases during neural differentiation.* J Neurochem, 2004. **91**(6): p. 1404-16.
9. Shenoy, S.K. and R.J. Lefkowitz, *β-arrestin-mediated receptor trafficking and signal transduction.* Trends in Pharmacological Sciences, 2011. **32**(9): p. 521-533.
10. Luttrell, L.M. and R.J. Lefkowitz, *The role of β-arrestins in the termination and transduction of G-protein-coupled receptor signals.* Journal of Cell Science, 2002. **115**(3): p. 455-465.
11. Benovic, J., et al., *Functional desensitization of the isolated beta-adrenergic receptor by the beta-adrenergic receptor kinase: potential role of an analog of the retinal protein arrestin (48-kDa protein).* Proceedings of the National Academy of Sciences of the United States of America, 1987. **84**(24): p. 8879 - 8882.
12. Shenoy, S. and R. Lefkowitz, *Trafficking patterns of beta-arrestin and G protein-coupled receptors determined by the kinetics of beta-arrestin deubiquitination.* The Journal of biological chemistry, 2003. **278**(16): p. 14498 - 14506.
13. Goodman, O., et al., *Beta-arrestin acts as a clathrin adaptor in endocytosis of the beta2-adrenergic receptor.* Nature, 1996. **383**(6599): p. 447 - 450.
14. Shenoy, S.K., et al., *β-arrestin-dependent, G protein-independent ERK1/2 activation by the β2 adrenergic receptor.* Journal of Biological Chemistry, 2006. **281**(2): p. 1261-1273.
15. Gurevich, V.V. and E.V. Gurevich, *GPCR Signaling Regulation: The Role of GRKs and Arrestins.* Frontiers in Pharmacology, 2019. **10**(125).
16. Eichel, K., D. Jullié, and M. von Zastrow, *β-Arrestin drives MAP kinase signalling from clathrin-coated structures after GPCR dissociation.* Nature cell biology, 2016. **18**(3): p. 303-310.
17. Latorraca, N.R., et al., *How GPCR phosphorylation patterns orchestrate arrestin-mediated signaling.* Cell, 2020. **183**(7): p. 1813-1825.e18.

18. Staus, D.P., et al., *Sortase ligation enables homogeneous GPCR phosphorylation to reveal diversity in β-arrestin coupling.* Proceedings of the National Academy of Sciences, 2018. **115**(15): p. 3834-3839.
19. Urano, D., et al., *Endocytosis of the seven-transmembrane RGS1 protein activates G-protein-coupled signalling in Arabidopsis.* Nat Cell Biol, 2012. **14**(10): p. 1079-88.
20. Chen, J.G., et al., *A seven-transmembrane RGS protein that modulates plant cell proliferation.* Science, 2003. **301**(5640): p. 1728-31.
21. Janetopoulos, C., T. Jin, and P. Devreotes, *Receptor-mediated activation of heterotrimeric G-proteins in living cells.* Science, 2001. **291**: p. 2408-2411.
22. Bradford, W., et al., *Eukaryotic G Protein Signaling Evolved to Require G Protein–Coupled Receptors for Activation.* Science Signaling, 2013. **6**(276): p. ra37-ra37.
23. Jones, J.C., et al., *Functional reconstitution of an atypical G protein heterotrimer and regulator of G protein signaling protein (RGS1) from Arabidopsis thaliana.* Journal of Biological Chemistry, 2011. **286**(15): p. 13143-13150.
24. Urano, D. and A.M. Jones, *"Round up the usual suspects": a comment on nonexistent plant G protein-coupled receptors.* Plant Physiol, 2013. **161**(3): p. 1097-102.
25. Watkins, J.M., et al., *Differential regulation of G protein signaling in Arabidopsis through two distinct pathways that internalize AtRGS1*. Science signaling, 2021. **14**(695).
26. Liang, X., et al., *Ligand-triggered de-repression of Arabidopsis heterotrimeric G proteins coupled to immune receptor kinases.* Cell research, 2018. **28**(5): p. 529-543.
27. Tunc-Ozdemir, M., et al., *Direct Modulation of Heterotrimeric G Protein-coupled Signaling by a Receptor Kinase Complex.* The Journal of biological chemistry, 2016. **291**(27): p. 13918-13925.
28. Tunc-Ozdemir, M. and A.M. Jones, *Ligand-induced dynamics of heterotrimeric G protein-coupled receptor-like kinase complexes.* PLOS ONE, 2017. **12**(2): p. e0171854.
29. Urano, D., et al., *Endocytosis of the seven-transmembrane RGS1 protein activates G-protein-coupled signalling in Arabidopsis.* Nat Cell Biol, 2012. **14**(10): p. 1079-1088.
30. Sun, Y., et al., *Structural basis for flg22-induced activation of the Arabidopsis FLS2-BAK1 immune complex.* Science, 2013. **342**(6158): p. 624-8.
31. Koller, T. and A.F. Bent, *FLS2-BAK1 extracellular domain interaction sites required for defense signaling activation.* PLoS One, 2014. **9**(10): p. e111185.
32. Shi, H., et al., *The retromer subunit Vps26 has an arrestin fold and binds Vps35 through its C-terminal domain.* Nat Struct Mol Biol, 2006. **13**(6): p. 540 - 548.
33. Lucas, M., et al., *Structural Mechanism for Cargo Recognition by the Retromer Complex.* Cell, 2016. **167**(6): p. 1623-1635 e14.
34. Collins, B., et al., *Structure of Vps26B and mapping of its interaction with the retromer protein complex.* Traffic, 2008. **9**(3): p. 366 - 379.
35. Oliviusson, P., et al., *Plant retromer, localized to the prevacuolar compartment and microvesicles in Arabidopsis, may interact with vacuolar sorting receptors.* Plant Cell, 2006. **18**(5): p. 1239-1252.
36. Watkins, J.M., et al., *Differential regulation of G protein signaling in Arabidopsis through two distinct pathways that internalize AtRGS1.* Sci Signal, 2021. **14**(695).
37. Leneva, N., et al., *Architecture and mechanism of metazoan retromer:SNX3 tubular coat assembly.* Sci Adv, 2021. **7**(13).
38. Liang, X., et al., *Ligand-triggered de-repression of Arabidopsis heterotrimeric G proteins coupled to immune receptor kinases.* Cell Res, 2018. **28**(5): p. 529-543.
39. Liang, X., et al., *Ligand-triggered de-repression of Arabidopsis heterotrimeric G proteins coupled to immune receptor kinases.* Cell research, 2018. **28**(5): p. 529-543.
40. Li, L., et al., *The FLS2-associated kinase BIK1 directly phosphorylates the NADPH oxidase RbohD to control plant immunity.* Cell Host & Microbe, 2014. **15**(3): p. 329-338.

41. D, C., et al., *A flagellin-induced complex of the receptor FLS2 and BAK1 initiates plant defence. .* Nature 2007. **448**: p. 497–500.
42. Venkatakrishnan, A.J., et al., *Molecular signatures of G-protein-coupled receptors.* Nature, 2013. **494**(7436): p. 185-94.
43. Sealfon, S.C., et al., *Related contribution of specific helix 2 and 7 residues to conformational activation of the serotonin 5-HT2A receptor.* J Biol Chem, 1995. **270**(28): p. 16683-8.
44. Gyombolai, P., et al., *Mutations in the 'DRY' motif of the CB1 cannabinoid receptor result in biased receptor variants.* J Mol Endocrinol, 2015. **54**(1): p. 75-89.
45. Yang, L.K., Z.S. Hou, and Y.X. Tao, *Biased signaling in naturally occurring mutations of G protein-coupled receptors associated with diverse human diseases.* Biochim Biophys Acta Mol Basis Dis, 2021. **1867**(1): p. 165973.
46. Sarma, P. and A.K. Shukla, *Resonating with the signaling bias of CXCR7.* Mol Cell, 2022. **82**(18): p. 3318-3320.
47. Rajagopal, S., et al., *Beta-arrestin- but not G protein-mediated signaling by the "decoy" receptor CXCR7.* Proc Natl Acad Sci U S A, 2010. **107**(2): p. 628-32.
48. Nguyen, H.T., et al., *CXCR7: a beta-arrestin-biased receptor that potentiates cell migration and recruits beta-arrestin2 exclusively through Gbetagamma subunits and GRK2.* Cell Biosci, 2020. **10**(1): p. 134.
49. Lou, F., et al., *An atypical heterotrimeric Galpha protein has substantially reduced nucleotide binding but retains nucleotide-independent interactions with its cognate RGS protein and Gbetagamma dimer.* Journal of biomolecular structure & dynamics, 2020. **38**(17): p. 5204-5218.
50. Clark, N.M. and R. Sozzani, *Measuring Protein Movement, Oligomerization State, and Protein-Protein Interaction in Arabidopsis Roots Using Scanning Fluorescence Correlation Spectroscopy (Scanning FCS).* Methods Mol Biol, 2017. **1610**: p. 251-266.
51. Tunc-Ozdemir, M. and A.M. Jones, *Ligand-induced dynamics of heterotrimeric G protein-coupled receptor-like kinase complexes.* Plos One, 2017. **12**(2).
52. Clark, N.M., et al., *Tracking transcription factor mobility and interaction in Arabidopsis roots with fluorescence correlation spectroscopy.* Elife, 2016. **5**.

List of Publications

Lou, F, Abramyan, TM, Jia, H, Tropsha, A, and Alan M. Jones (2019) An atypical heterotrimericGα protein has substantially reduced nucleotide binding but retains nucleotide-independent interactions with its cognate RGS protein and Gβγ dimer. *J. Biological and Structural Dynamics Dec 23;1-15* 10.1080/07391102.2019.1704879 also on *BioRxiv* doi.org/10.1101/795088

Cao-Pham AH, Urano D, Ross-Elliott TJ, Jones AM (2018) Nudge-Nudge, WNK-WNK (kinases), Say No More? Invited Tanksley Review *New Phytologist* **220**: 35-48

Huang J-P, Tunc-Ozdemir M, Chang Y and Jones AM (2015) Functional overlap between AtRGS1- and AtHXK1-dependent sugar signaling in Arabidopsis. *Frontiers in Plant Science* 13;6:851. doi: 10.3389/fpls.2015.00851 PMCID: PMC4602111

Li, B, Makino,S, Beebe, ET, Urano, D, Aceti, DJ, Misenheimer, TM, Peters, J, Fox, BG, Jones, AM (2016) Cell-free translation and purification of *Arabidopsis thaliana* regulator of G protein signaling 1. *Protein Expression and Purification* **126**: 33-41 doi: 10.1016/j.pep.2016.04.016 PMCID: PMC5594927

Urano, D, Colaneri, A, Jones, AM (2014) Gα modulates salt-induced cellular senescence and cell division in rice and maize. *J. Expt Botany* **65**: 6553–6561 doi: 10.1093/jxb/eru372 PMCID: PMC4246186

Liao K-L, Melvin, CE, Sozzani R, Jones RD, Elston TC, Jones AM (2017) Dose-Duration Reciprocity for G protein activation: Modulation of kinase to substrate ratio alters cell signaling. *PLoS One* *12*, e0190000 doi: 10.1371/journal.pone.0190000 PMCID: PMC5635846

Urano D, Leong R, Wu TY, Miura K, Jones AM Quantitative morphological phenomics of rice G protein mutants portend autoimmunity disease. *Developmental Biology*

Tunc-Ozdemir, M Jones AM (2017) BRL3 and AtRGS1 cooperate to fine tune growth inhibition and ROS activation. *PLoS ONE* **12**(5):e0177400. doi: 10.1371 PMCID: PMC5436702

Wolfenstetter, S Chakravorty, D, Kula, R, Urano, D, Trusov, Y, Sheahan, MB, McCurdy, DW, Assmann, SM, *Jones, AM, Botella, JR (2015) Evidence for an unusual trans- membrane configuration of AGG3, a class C Gγ subunit, of Arabidopsis. *The Plant Journal* **81**(3):388-98 *corresponding author doi: 10.1111/tpj.12732 PMCID: PMC4334566

Liao, K-L, Jones, RD, McCarter, P, Tunc-Ozdemir, M, Draper, JA,Elston, TC, Kramer, D, Jones, AM (2017) A shadow detector for photosynthesis efficiency. *J. Theoret. Biol*. **414**: 231-244 **doi**: 10.1016/j.jtbi.2016.11.027.

Urano, D, Maruta, N, Trusov, Y, Stoian, R, Liang, Y, Jaiswal, DK, Thung, L, Botella, JR, and Jones, AM (2016) Saltational evolution of the heterotrimeric G protein signaling mechanisms in the plant kingdom. *Science Signaling* Vol 9, Issue 446 20 September 2016 featured on the cover **doi**: 10.1126/scisignal.aaf9558

Urano, D, Czarnecki, O, Wang, X, *Jones, AM, Chen, J-G (2015) Arabidopsis RACK1 phosphorylation by WNK8 kinase. *Plant Physiol*. **167**: 507–516 *corresponding author DOI: https://doi.org/10.1104/pp.114.247460 PMCID: PMC4326752

Tunc-Ozdemir, M, Urano, D, Jaiswal, DK, Clouse, SD, Jones, AM (2016) Direct activation of a heterotrimeric G protein by a receptor kinase complex. *J. Biol Chem*. **291**: 13918-13925 DOI: 10.1074/jbc.C116.736702 PMCID: PMC4933153

Jaiswal, DK, Werth, EG, McConnel, EW, Hicks, LM, Jones, AM 2015 Time-dependent, glucose-regulated Arabidopsis Regulator of G-protein Signaling 1 network. *Curr. Plant Biol*. (on-line 23Dec2015) doi.org/10.1016/j.cpb.2015.11.002

Tunc-Ozdemir, M, Jones, AM (2017) Ligand-induced dynamics of a heterotrimeric G protein-coupled receptor kinase complex *PLoS ONE* **12**: e0171854 https://doi.org/10.1371/journal.pone.0171854 PMCID: PMC5302818

Urano, D, Dong, T, Bennetzen, JL, Jones, AM (2015) Adaptive evolution of signaling partners. *Mol Biol. Evol*. advance access Jan 6 doi:10.1093/molbev/msu404 PMCID: PMC4379405

Fu, Y, Lim, S, Urano, D, Phan, NG, Elston, TC, Jones, AM (2014) Reciprocal encoding of

signal intensity and duration in the glucose-sensing circuit *Cell* **156**: 1084-1095 doi: 10.1016/j.cell.2014.01.013 PMCID: PMC4364031

Mudgil, Y, Karve, A, Teixeira, PJPL, Colaneri, A, Yang, J, Jiang, K, Tunc-Ozdemir, M, and Jones, AM (2016) Photosynthate regulation of the root system architecture mediated by the heterotrimeric G protein complex. *Frontiers in Plant Science* **7**: article 1255 doi.org/10.3389/fpls.2016.01255 PMCID: PMC4997095

Urano, D, Jackson, D and Jones AM (2015) A null G protein alpha mutation confers prolificacy in maize. *J. Expt Botany* doi :10.1093/jxb/erv215 PMCID: PMC4507758

Liang, Y, Gao, Y, Jones, AM (2017) Extra Large G-protein interactome reveals multiple stress response function and partner-dependent XLG subcellular localization. *Frontiers in Plant Sci*. doi: 10.3389/fpls.2017.01015

Liang, Y, Urano, D, Gao, Y, Hedrick, TL, Jones, AM (2017) A nondestructive method to estimate the chlorophyll content of *Arabidopsis* seedlings *Plant Methods* **13**:26. doi: 10.1186/s13007-017-0174-6 PMCID: PMC5391588

Tunc-Ozdemir, M., Liao, K-L, Jones, AM (2018) Long-distance communication in Arabidopsis involving a self-activating G protein. Feb 26 DOI: 10.1002/pld3.37

Colaneri, AC, Tunc-Ozdemir, M, Huang, JP, Jones, AM (2014) Growth attenuation under saline stress is mediated by the heterotrimeric G protein complex. *BMC Plant Biology* **14**:129 doi: 10.1186/1471-2229-14-129 PMCID: PMC4061919

Li, B, Urano, D, Mowrey, DD, Dokholyan, NV, Torres, MP, Jones, AM (2018) Tyrosine phosphorylation switching of a G protein substrate. *J. Biol Chem*. **293**(13):4752-4766. doi: 10.1074/jbcRA117.000163

Escudero, V Jordá, J, Sopeña-Torres, S, Mélida, H, Muñoz-Barrios, A, Swami, S, Alexander, D, McKee, LS, Sánchez-Vallet, A, Bulone, V, Jones, AM, Molina, A (2017) Alteration of cell wall xylan acetylation triggers defensive responses that counterbalance the immune deficiencies of plants impaired in the β subunit of the

heterotrimeric G protein. *Plant Journal* 92(3):386-399. doi: 10.1111/tpj.13660 PMCID: PMC5641240